

Quantitatively Mapping the Distribution of Intrinsic Acid Sites in Mordenite Zeolite by High-Field ^{23}Na Solid-State Nuclear Magnetic Resonance

Benhan Fan, Wenna Zhang, Pan Gao, Guangjin Hou, Rongsheng Liu, Shutao Xu,* Yingxu Wei, and Zhongmin Liu



Cite This: *J. Phys. Chem. Lett.* 2022, 13, 5186–5194



Read Online

ACCESS |



Metrics & More

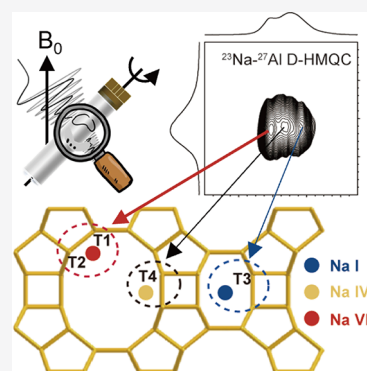


Article Recommendations



Supporting Information

ABSTRACT: It is of great significance to accurately quantify the Brønsted acid sites (BASs) at different positions of mordenite (MOR) zeolite. However, H-MOR obtained from Na-MOR can hardly avoid dealumination under hydrothermal conditions, which causes difficulty in the acid characterization. Herein, ^{23}Na - ^{27}Al D-HMQC was performed combined with high-field ^{23}Na MQ MAS NMR and DFT calculation, which provided an unambiguous attribution of the ^{23}Na chemical shifts and further helped to improve the resolution of ^{27}Al MAS NMR. By fitting the ^{23}Na and ^1H MAS NMR spectra of Na/H-MOR, the intrinsic BAS contents in different T-sites were measured by characterizing the location and content of sodium ions. These Na/H-MOR zeolites with various acid distributions were used for DME carbonylation and showed that the amount of BASs in the T3 site was proportional to the activity of carbonylation. This study provides a new method for investigating the intrinsic acid properties of zeolites.



Dimethyl ether (DME) carbonylation to methyl acetate (MA) over zeolites and MA further hydrogenation to ethanol have attracted great attention in recent years mainly because these processes provide a new way to yield high-value chemicals and fuel from C1 resources and, at the same time, to realize the clean utilization of coal resources.¹ Since 2006, mordenite (MOR) zeolite has been first reported to have excellent DME carbonylation activity.² In the following decades, continuous efforts have been made on the modification of MOR zeolite to improve the activity and stability.^{3–10} In January 2017, the world's first demonstration project for the production of ethanol (>100,000 t per year) from coal by DME carbonylation, developed by the Dalian Institute of Chemical Physics of the Chinese Academy of Science, was proved completely successful in Shaanxi province of China.

MOR zeolite has four nonequivalent tetrahedral T-sites, and the topology structure is characterized by parallel twelve-membered-rings (12-MRs, $6.5 \times 7 \text{ \AA}$) and eight-membered-rings (8-MRs, $2.6 \times 5.7 \text{ \AA}$) direct channels along the 001 direction which are connected by 8-MR side pockets (SPs, $3.4 \times 4.8 \text{ \AA}$) along the 010 direction.^{1,11} The reaction mechanism of DME carbonylation on MOR zeolite had been widely studied by multiple approaches such as IR,^{12,13} solid-state NMR,^{14,15} and theoretical calculation.^{16–20} It is widely accepted that the 8-MR side pockets serve as critical reactive centers and the 12-MR channel provides diffusion paths.^{21–23} To accurately identify the active centers, many researchers had studied the 12-MR and 8-MR individually with the methods of

pyridine modification^{3,24} and sodium ion poisoning.^{21,25–28} The molecular diameter of pyridine is 5.3 \AA , which is larger than the size of the SP window ($3.4 \times 4.8 \text{ \AA}$), so the pyridine molecule could hardly pass through the SP and only affects the Brønsted acid sites (BASs) in the 12-MR.^{5,13,29} Recently, our group found that the existence of defects in the SP would enlarge the window of the 8-MR, so that pyridine was able to pass through the 8-MR and would influence the quantitative accuracy of the BASs in the 8-MR.⁴ Na^+ ions could preferentially exchange protons in the 8-MR compared to the 12-MR, which was proved by the IR method.³⁰ A certain exchange degree of Na/H-MOR (mostly 45% approximately) was considered to be the target sample for which most of the BASs were located in the 12-MR and the BASs in the 8-MR were poisoned by Na^+ ions.¹⁴ However, this method hardly excluded a certain number of BASs still located in the 8-MR. Therefore, accurate determination of the numbers and locations of acid sites is of great significance to make clear the specific catalytic effects of different MOR channels, even for different T-sites.

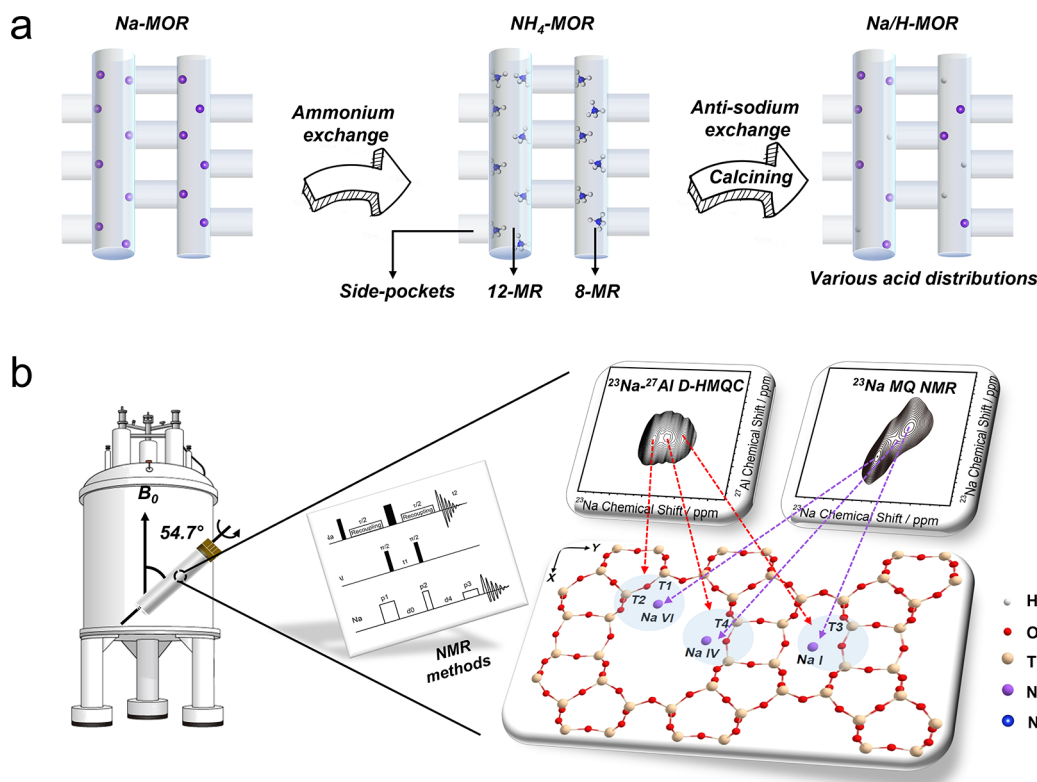
Received: March 31, 2022

Accepted: May 31, 2022

Published: June 6, 2022



Scheme 1. (a) Sample Preparation Method^a (b) High-Field ^{23}Na MQ MAS NMR and ^{23}Na - ^{27}Al D-HMQC Were Combined to Distinguish Different Sites of Na^+ Ions Located at Na VI, Na IV, and Na I^b



^a $\text{NH}_4\text{-MOR}$ was obtained from NaMOR with the thorough-paced ammonium exchange method and then anti-exchanged by various concentrations of sodium nitrate solution, at last calcinating to get the Na/H-MOR with the characterization of various acid distributions. ^b ^{23}Na - ^{27}Al D-HMQC also improved the resolution of different Al T-sites considering the spatial proximity of Na^+ ions and Al atoms in different T-sites.

Adsorption of probe molecules and characterization by the IR or NMR method have been proven to be a powerful tool for exploring the acidities of zeolites.^{31–34} However, the existing methods of acid characterization in MOR zeolite, such as measuring the total BASs by quantitative ^1H MAS NMR or identifying the acid contents in the 12-MR and 8-MR by IR or adsorption of probe molecules, find it difficult to obtain an accurate measurement of the acid amounts in the different T-sites.^{21,27,35,36} Meanwhile, H-MOR acquired from Na-MOR via a sequence of steps, such as ion-exchanging and calcination, can hardly avoid dealumination during the procedure, which causes difficulty in differentiating and quantifying the BASs located in various positions. It should be noted that the extra-framework Na^+ ions not only play the same role as protons to balance the negative charge of the aluminum oxygen tetrahedron but also improve the stability of the zeolite framework. The locations of sodium ions in dehydrated MOR had been characterized by various methods, and the acknowledged three possible sites are Na I, Na IV, and Na VI which are located in the 8-MR channel, side pockets, and 12-MR channel, respectively.^{37,38} Therefore, the amount of acid in different sites could be reflected by measuring the contents of Na^+ ions at different positions, which can be developed as a new method for acid characterization.

The solid-state NMR technique is a powerful tool to investigate the structural framework and extra-framework information (such as Al atoms, protons, and Na^+ ions) in multiple kinds of molecular sieves.^{39–44} In this work, a gradient

of Na/ $\text{NH}_4\text{-MOR}$ samples were elaborately prepared by controlling the ion-exchanged conditions and then calcined to obtain Na/H-MOR samples without dealumination (Scheme 1a). High-field ^{23}Na MQ MAS NMR, ^{23}Na - ^{27}Al D-HMQC, and DFT calculation were combined to distinguish different sites of Na^+ ions located at Na VI, Na IV, and Na I (Scheme 1b). These Na/H-MOR zeolites with different BAS concentrations and distributions were adopted to investigate the different acid sites by quantitative ^1H and ^{23}Na MAS NMR and then evaluated by DME carbonylation to gain an in-depth understanding of the roles of different MOR T-sites. These results demonstrated that the intrinsic acidity could be quantitatively mapped by ^{23}Na NMR excluding the effect of dealumination, which exhibits great potential for various applications including acidic characterizations and adjustment at the atomic level.

Monitoring the Evolution of Protons in Sodium-Exchanged MOR Zeolite. Herein, $\text{NH}_4\text{-MOR}$ was obtained from NaMOR with the thorough-paced ammonium exchange method and then anti-exchanged by various concentrations of sodium nitrate solution. The samples are defined as $x\text{Na}/(100 - x)\text{NH}_4\text{-MOR}$ (x represents the exchange degree of sodium ions in atom percent which was obtained by XRF, and the values are 28, 39, 51, and 75, respectively), and these further deammoniated samples are defined as $x\text{Na}/(100 - x)\text{H-MOR}$. The detailed sample information is shown in Table S1. The similar XRD patterns (Figure S3) of the samples indicate the crystallinity of MOR zeolites is well maintained during the

initial exchange from Na^+ to NH_4^+ type and the reverse exchange from NH_4^+ to partial Na^+ type. The ^{27}Al MAS NMR spectrum of H-MOR (Figure S4) shows an obvious signal at 0 ppm, which is attributed to the extra-framework Al with an octahedral coordination state, and the primary signal at approximately 55 ppm is assigned to the tetrahedrally coordinated Al in the zeolite framework, illustrating that the dealumination of H-MOR with a low Si/Al ratio is inevitable in the process of deammoniation.^{45–49} In the ^{27}Al MAS NMR spectra of all the Na^+ ion-exchanged zeolites calcined at 473, 673, and 773 K (Figure S5), only a single peak at 55 ppm can be seen and no signal appeared at 0 ppm, demonstrating the presence of sodium ions can effectively avoid the dealumination during the calcining process. The ^1H MAS NMR spectra of all the Na^+ ion-exchanged samples heated at different temperatures are recorded (Figure S6). Noticeably, four signals at 6.4, 3.8, 2.6, and 1.8 ppm are observed, which are unambiguously assigned to undecomposed ammonium (NH_4^+), bridging hydroxyls (BASs), extra-framework aluminum hydroxyls (Al-OH), and silicon hydroxyls (Si-OH), respectively.^{50–53} These $x\text{Na}/(100-x)\text{NH}_4$ -MOR zeolites are first heated at 473 K, and the primary resonances at 6.4 ppm are assigned to undecomposed NH_4^+ species. A negligible signal of BASs at 3.8 ppm and unavoidable external surface silanol groups at 1.8 ppm can be observed, which means that most of the adsorbed water molecules are removed and a very small number of NH_4^+ species are decomposed at this temperature. With the temperature increasing to 673 K, the integral area of 6.4 ppm in the ^1H NMR spectrum decreases significantly because a large number of NH_4^+ ions are removed, resulting in corresponding BASs being generated. It is notable that there are still residual NH_4^+ species existing after heating at 673 K, indicating the complete deamination needs a higher temperature.^{54,55} With increasing the temperature to 773 K, all the NH_4^+ signals disappear and the signals from bridging hydroxyls become intensified, demonstrating the complete decomposition of NH_4^+ from $x\text{Na}/(100-x)\text{NH}_4$ -MOR. ^1H MAS NMR measurement of the obtained $x\text{Na}/(100-x)\text{H}$ -MOR is performed for the quantitative data (Table S2). During the whole process, the content of non-active Si-OH is maintained constantly, illustrating no occurrence of Na ion exchange with the protons from silanol groups. On the other hand, when a series of Na^+ -exchanged MOR zeolites are compared in Figure S6, the peak intensities of NH_4^+ and BAS decreased significantly accompanied by the increase of Na^+ , which proves that Na^+ took the proton for compensating the negatively charged MOR framework.

Mapping the Distributions of Sodium Ions in Different Positions. ^{23}Na MAS NMR spectroscopy is employed to determine the initial position of the Na ions. ^{23}Na (a spin 3/2 nucleus) is greatly affected by the second-order quadrupole interactions, resulting in a concomitant lower resolution such as broadening or a distorted signal which is represented in the NMR spectrum. The higher magnetic field could represent a better resolution than the lower field by suppressing the effects of second-order quadrupolar broadening which is mainly because the quadrupole interaction is inversely proportional to the strength of the magnetic field.

The Na-MOR zeolite is dehydrated at 773 K, and then, ^{23}Na MAS NMR and ^{23}Na MQ MAS NMR spectra are acquired at 14.1 and 18.8 T (Figure 1). There are two distinct peaks at -18 and -30 ppm in the one-dimensional spectrum of ^{23}Na MAS NMR (14.1 T). The second-order quadrupole

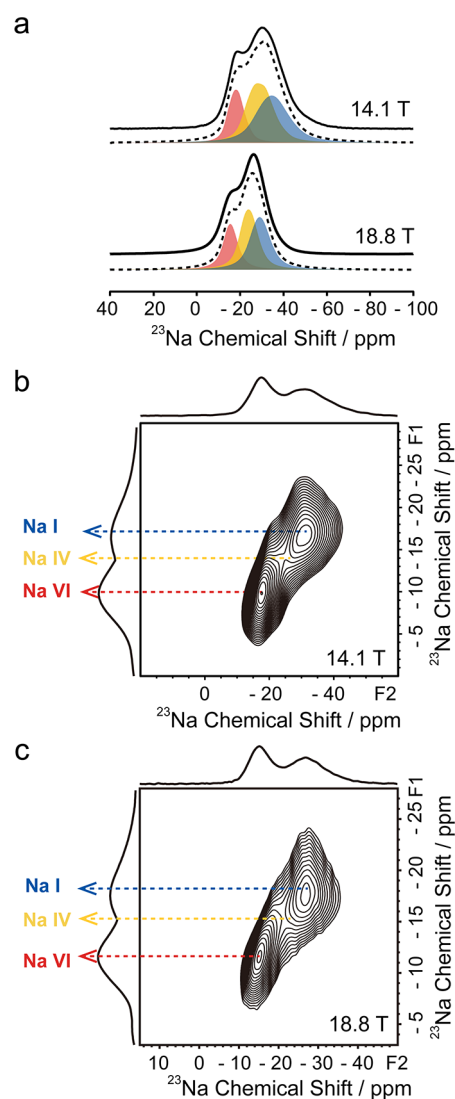


Figure 1. (a) ^{23}Na MAS NMR spectra of Na-MOR acquired at 14.1 and 18.8 T, respectively. 2D ^{23}Na MQ MAS NMR spectra of Na-MOR zeolite acquired at 14.1 T (b) and 18.8 T (c). Na-MOR was dehydrated at 773 K before the NMR experiments.

interactions are inversely proportional to the strength of the magnetic field. To improve the resolution, the spectrum at the higher field (18.8 T) is adopted which shows narrower lines and chemical shifts of the two distinct peaks moved to the relatively lower field at -16 and -27 ppm, respectively. These two signals cannot be completely separated directly in the ^{23}Na MAS NMR due to the second-order quadrupole interactions; therefore, they need to be further distinguished by two-dimensional (2D) ^{23}Na MQ MAS spectra as shown in Figure 1b and c. A pioneering work reported a series of Na ions observed in dehydrated zeolites (NaY, NaEMT, NaZSM-5, and NaMOR) through ^{23}Na triple-quantum (3Q) MAS NMR spectroscopy at 11.75 T.⁴³ Due to the lower magnetic field, three Na sites in MOR zeolite were not differentiated by ^{23}Na MQ MAS NMR.

By slicing and fitting the spectra at different isotropic dimensions (F1) which are parallel to the acquisition dimension (F2), significant NMR parameters such as the quadrupolar coupling constant (C_Q), isotropic chemical shift (δ_{iso}), and asymmetry parameter (η) are obtained. Utilizing

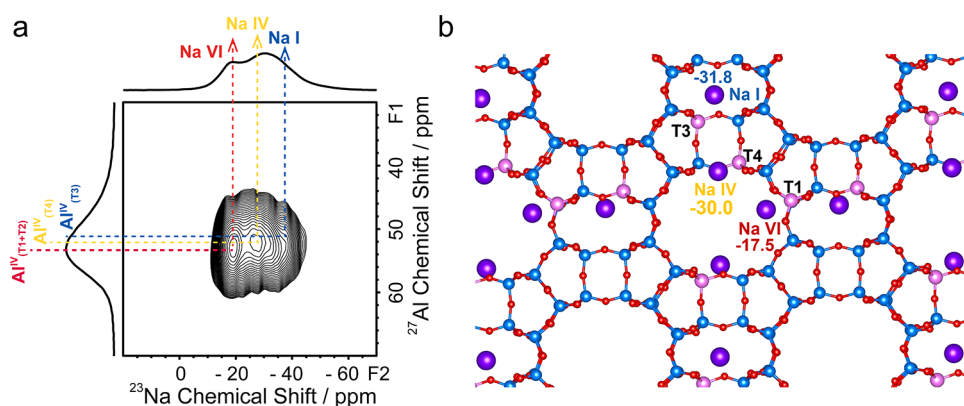


Figure 2. (a) 2D ^{23}Na - ^{27}Al *D*-HMQC MAS NMR spectrum of Na-MOR acquired at 14.1 T; the corresponding ^{23}Na and ^{27}Al single pulse MAS NMR spectra are displayed on the top and left of the 2D spectrum. (b) DFT calculations of the ^{23}Na NMR chemical shifts of the different sodium ions sites in Na-MOR.

fitting the slice data in the MQ MAS NMR spectra acquired at 14.1 T (Figure 1b), the signal at the F1 dimension with chemical shift (δ_{iso}) at -13 ppm with a smaller P_Q (2.4 MHz) is ascribed to Na VI located in the 12-MR main channel along the 001 direction and also in the center of the 6-MR surrounded by four T1 and two T2 atom sites (Figure S7).⁴³ The other two signals with the δ_{iso} at approximately -20 and -25 ppm are attributed to Na IV and Na I, respectively. Evidence of the signal attribution is given below. To validate the fitting veracity, the MQ MAS NMR spectrum of NaMOR is acquired at a higher field (Figure 1c). Three signals with similar δ_{iso} at approximately -12 , -19 , and -24 ppm along the F1 dimension combining the same parameters of P_Q and η prove the correctness and reasonableness of the slice fitting. Then the 1D ^{23}Na MAS NMR spectrum of NaMOR is fitted using the same parameters extracted from the ^{23}Na MQ MAS NMR spectrum, and three different integral areas could similarly represent the amount of sodium in different positions. The quantitative sodium contents are listed in Table S3. From the fitness of the NaMOR sample, the quantitative distinguishment of the initial position of Na^+ can be obtained, with approximately 21.35% of Na^+ located in Na VI, 39.46% of Na^+ located in Na IV, and the remaining 39.19% of Na^+ located in Na I.

Heteronuclear correlation experiments of ^{23}Na - ^{27}Al *D*-HMQC and *D*-RINEPT on $\text{Na}_2\text{CO}_3/\gamma\text{-Al}_2\text{O}_3$ catalyst give a new way to detect different Na sites adjacent to Al atoms.⁵⁶ To the best of our knowledge, the relationship between extra-framework cations (sodium ions) and active sites (aluminum atoms) in zeolites had been rarely researched through the interaction of two quadrupolar nuclei ^{23}Na and ^{27}Al . In our recent work, high-field (18.8 T) ^{27}Al MAS NMR and ^{27}Al MQ MAS NMR were used conjointly to explore the MOR zeolite with higher Si/Al ratio (47.5) which was obtained by the low-pressure SiCl_4 treatment method. Four nonequivalent T-sites were clearly differentiated in the ^{27}Al MQ MAS NMR spectrum, and the signals in the ^{27}Al MAS NMR from low field to high field were uncontroversially attributed to Al atoms located in T2, T1, T4, and T3, respectively.⁶

In order to provide the evidence of ^{23}Na signal attribution, the ^{23}Na - ^{27}Al *D*-HMQC MAS NMR spectrum of Na-MOR is adopted (Figure 2a), and three well distinguished correlation peaks can be observed. From the ^{27}Al dimension (F1), the signal at 53 ppm is attributed to Al T-sites of T1 and T2. Correspondingly, the signals at 52 and 50.5 ppm are attributed

to the Al T-sites of T4 and T3, which is consistent with our previous work.⁶ Due to the spatial proximity of the Na^+ and T-sites of the Al atom (Figure S7), three signals from the ^{23}Na dimension (F2) which correspond to the three peaks of the ^{23}Na MQ MAS NMR spectrum are attributed to the Na VI, Na IV, and Na I sites from low field to high field. ^{27}Al MAS NMR and ^{27}Al MQ MAS NMR spectra are also acquired at 14.1 and 18.8 T (Figure S8). From the ^{27}Al MAS NMR spectra of Na-MOR under two different magnetic fields, only one asymmetrical peak representing framework tetrahedrally coordinated Al can be observed. It is difficult to distinguish the different T-sites from the ^{27}Al MQ MAS NMR spectrum at 14.1 and 18.8 T. The low resolution in ^{27}Al MQ MAS NMR is possibly ascribed to the lower Si/Al ratio (6.5). The heteronuclear correlation between two quadrupolar nuclei provides a new opportunity to improve the resolution of different Al T-sites by observing the spatially adjacent Na-Al species in other zeolites.

DFT calculation (Figure 2b) is also performed to verify the location of Na ions and the assignment of their signals in NMR spectra. During the calculation of NMR parameters, an appropriate geometry model of the zeolite has a significant effect on the NMR shielding of Na^+ in cationic sites. Meanwhile, it is necessary to focus on the Al distributions in optimizing the theoretical computation model. It has been proven that different topological zeolites, or even the same topological zeolite with same Si/Al ratio, would bring different Al distributions by different synthesis methods.^{57–61} Therefore, modeling the Al distribution approximate to the actual sample could increase the reliability of the DFT calculation. However, it still needs to be acknowledged that the Al distribution of actual samples is more complex and difficult to represent by a single calculation model. This also leads to errors between theoretical calculations and NMR experiments. Therefore, the DFT calculation is only a supplementary method to verify the experiment results.

The Al distribution of the actual sample is taken into account in the calculation of ^{23}Na chemical shifts. It is well-known that the Al-O-Si-O-Al chains exist in the zeolite with the lower Si/Al ratio.^{62,63} To prove the existence of the Al-O-Si-O-Al chains, the ^{29}Si MAS NMR spectrum of NaMOR (Figure S9) is adopted. The two main peaks at -105 and -111 ppm are attributed to Si1Al and Q^4 (0Al), respectively, and the signal at -100 ppm is attributed to Q^3 . The noticeable signal at -98 ppm is assigned to Si2Al (Al-O-Si-O-Al, Al pair), which

means the Al pair species exist in the parent Na-MOR.⁶⁴ The Si/Al calculated by ²⁹Si MAS NMR is 6.43, which is very close to the result of the X-ray fluorescence (XRF) method (6.5). From the quantitative results from the ²³Na MAS NMR spectrum of Na-MOR, the ratio of sodium ions located in Na VI, Na IV, and Na I is 1:2:2, approximately. Based on the above results, the position and content of Na⁺ are considered in the structural optimization. It is proposed that Al has less probability to occupy the T2 site, which is proved by multiple theoretical calculation methods.^{65–67} To simplify the model of this work, Al atoms are only considered in the T3, T4, and T1 sites owing to the lowest proportion of the T2 site.⁶⁸ The distribution of different Al sites (T3:T4:T1 = 2:2:1) was obtained from the integral quantitation from ²³Na MAS NMR (approximately Na I:Na IV:Na VI = 2:2:1). In a unit cell of the Na-MOR model (Figure S10), five Al (T1 + 2T3 + 2T4) atoms and five Na (Na VI + 2Na I + 2Na IV) ions are used for the calculation of ²³Na chemical shifts, and the calculated NMR parameters (δ_{iso} , C_{Q} and η) are listed in Table S4. The calculated isotropic ²³Na chemical shifts of Na VI (−17.5 ppm), Na IV (−30 ppm), and Na I (−31.8 ppm) are in the same order with the signal assignments of ²³Na MAS NMR and ²³Na MQ MAS NMR spectra from low to high field (Table S3). However, there are still relatively differences between the calculated values (δ_{iso} , C_{Q} and η) and the experimental measurements, and several possible reasons are as follows. The mobility of Na ions in the actual sample will affect the quadrupolar interaction of ²³Na nuclei and further influence the NMR parameters. The parameters δ_{iso} , C_{Q} and η which were acquired and fitted from the slices of the ²³Na MQ MAS NMR spectrum just represent the average values of Na ions in different positions of the complicated actual sample. The DFT calculation provides an approximate theoretical model which has some difference compared to the actual sample, so the values obtained are only for reference but can also represent the unique properties of Na ions in different chemical environments.

Correlation between Acidity and Catalytic Performance for DME Carbonylation. The negative charge of the zeolite framework comes from AlO_4^- , which is compensated by equilibrium ions such as Na⁺ or protons. Therefore, the intrinsic BAS contents in different T-sites were measured and deduced by characterizing the location and content of sodium ions. The ²³Na MAS NMR spectra of $x\text{Na}/(100-x)\text{H-MOR}$ and fitting curves of the ²³Na MAS NMR spectra are shown in Figure 3a, and the quantitative data of sodium ions in different sites are summarized in Table S5. For visualization exhibiting the changes of sodium ions at different positions, the quantitative sodium contents are described in bar chart style, which is shown in Figure 3b. For the 28Na/72H-MOR sample, almost all the Na⁺ ions are located in the Na IV and Na I positions, while only fewer Na⁺ ions are located in the Na VI position. For the 51Na/49H-MOR sample, the content of sodium ions in the Na VI site is remarkably increased, illustrating Na⁺ ions located in the 12-MR main channel inevitably occur in the process of sodium ion exchange. The content of Na⁺ ions in different sites is increasing synchronous with the exchange degree and the increasing amplitude has no difference for the different sites. The most discussed sample with all the Na⁺ ions only located in the 8-MR and all the BASs located in the 12-MR is hard to prepare by the Na⁺ exchange method. Na⁺ ions preferential located in the 8-MR have been proven in the Na exchange process.³⁰ So in the fitting curves of

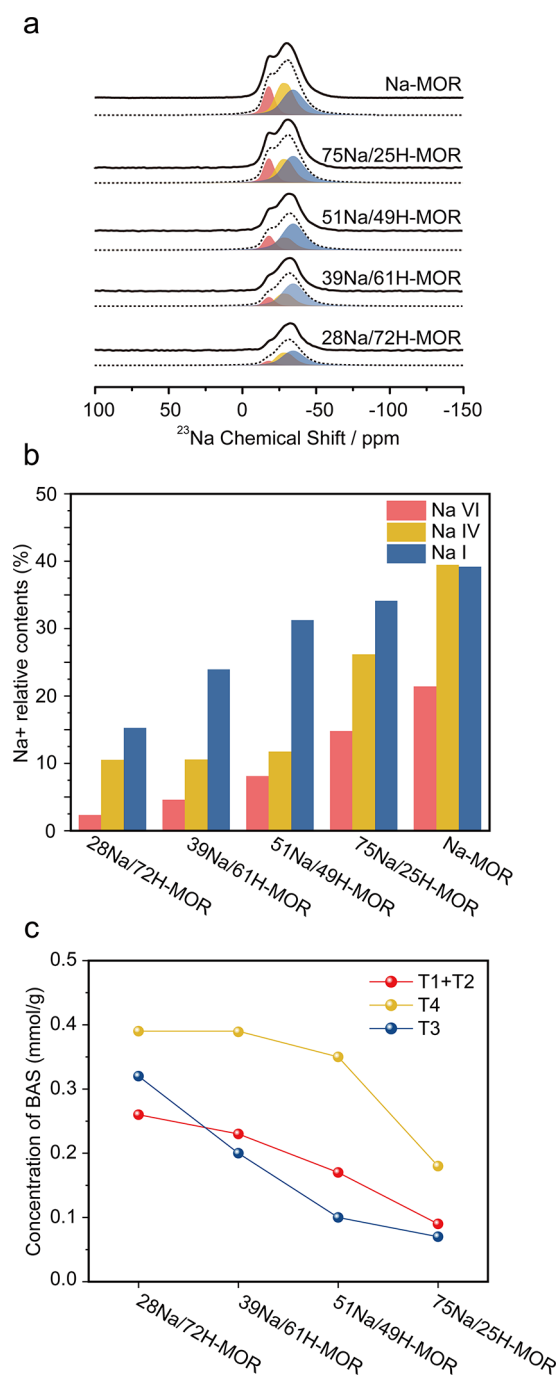


Figure 3. (a) ²³Na MAS NMR spectra and their deconvolutions of $x\text{Na}/(100-x)\text{H-MOR}$ zeolites acquired at 14.1 T. (b) Na⁺ relative contents in different positions of $x\text{Na}/(100-x)\text{H-MOR}$ zeolites. (c) Concentration of BASs in different T-sites of $x\text{Na}/(100-x)\text{H-MOR}$ which were heated at 773 K.

the ²³Na MAS NMR spectrum from 28Na/H-MOR, the largest area represents the Na⁺ located in the 8-MR; hence, the signal of ²³Na MAS NMR at higher field is undisputedly attributed to the Na I site, and corresponding, the signal in the middle is attributed to the Na IV site, which also proves the correctness of the signal attribution of ²³Na MAS NMR. The total acid contents of $x\text{Na}/(100-x)\text{H-MOR}$ are acquired by ¹H MAS NMR spectra, and quantitative information on sodium ions in different positions are also obtained by fitting ²³Na MAS NMR spectra. Due to the spatial proximity of

sodium ions and different Al sites, the contents of Na ions located at Na VI, Na IV, and Na I could also represent the protons of H-MOR which are located in the T1 + T2, T4, and T3 sites, in the case that dealumination can be avoided during the ion exchange. The numbers of protons and Na ions at different sites are explicit by the integral areas of ^1H and ^{23}Na MAS NMR spectra. Therefore, the BASs of T1 + T2, T4, and T3 in $x\text{Na}/(100 - x)\text{H-MOR}$ could be precisely calculated by the difference between the number of protons and sodium ions of the partially Na^+ -exchanged MOR, which are shown in Table S6 and Figure 3c.

All the $x\text{Na}/(100 - x)\text{H-MOR}$ zeolites are employed as catalysts for DME carbonylation, and DME conversion and MA selectivity are evaluated as shown in Figure 4a. There is an

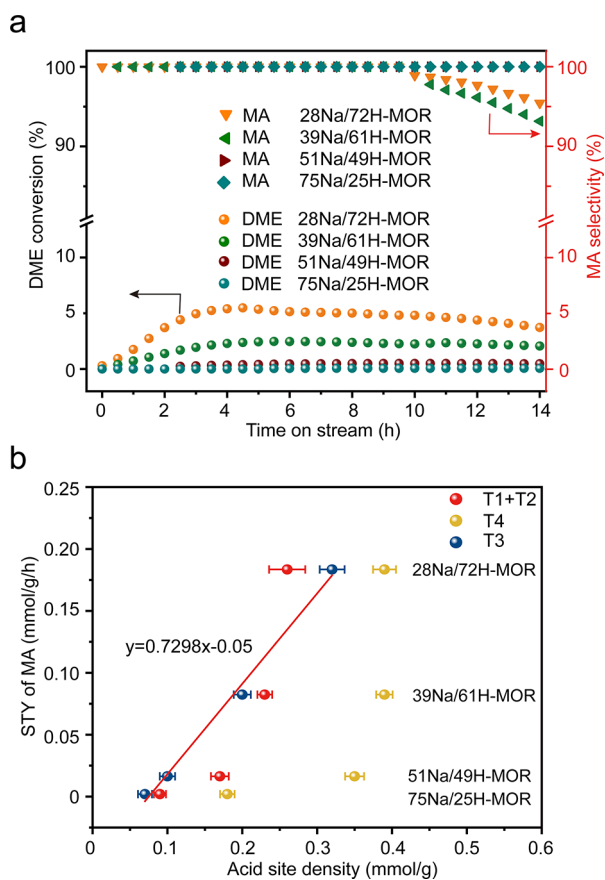


Figure 4. (a) Catalytic performance for DME carbonylation over $x\text{Na}/(100 - x)\text{H-MOR}$. (b) STY of MA plotted against the acid site density in T1 + T2 (red point), T4 (yellow point), and T3 (blue point) sites of MOR zeolites. Reaction conditions: 473 K, 2 MPa, $\text{DME}/\text{CO}/\text{N}_2 = 5/35/60$, $\text{WHSV} = 1500 \text{ mL/h/g}$. The DME conversion from high to low corresponds to the samples 28Na/72H-MOR, 39Na/61H-MOR, 51Na/49H-MOR, and 75Na/25H-MOR.

induction period for DME carbonylation with a very slow increase in conversion rate due to the formation of surface methoxy species from the DME reaction over BASs.¹⁵ After the induction period, the conversion rate of DME reaches a relatively stable platform for several hours and then declines gradually. The deactivation is due to coke formation from the methanol-to-hydrocarbons (MTH) reactions over BASs in the 12-MR and, thus, suppressed DME carbonylation in the 8-MR.^{16,18} During the whole reaction procedure except the deactivation period, nearly 100% MA selectivity can be

achieved. With the increase of Na content in MOR zeolite, DME conversion decreases gradually, which means that the acidic sites are essential for the reaction of DME carbonylation. For further understanding of the relationship between BASs of different positions and catalytic activity, acid amounts in T1 + T2, T4, and T3 corresponding to the space-time yield (STY) of MA are listed in Figure 4b. Focusing on the three samples (28Na/72H-MOR, 39Na/61H-MOR, and 51Na/49H-MOR) with observable catalytic activity, an interesting consequence could be observed that the STY of MA is linearly proportional to the number of acid site density in the T3 sites, while the STY of the MA variation shows no direct relation with the acid site density of the T1 + T2 and T4 sites. This indicates that the acid sites in the T3 sites are essential to DME carbonylation; moreover, it also experimentally demonstrates that the acid site in the T3 site is the active center of the carbonylation reaction, which had been proposed by the theoretical calculation.¹⁶

In summary, the locations and contents of extra-framework cations such as protons and Na^+ ions in a series of Na-exchanged MOR zeolites are investigated thoroughly by multiple NMR methods mainly including ^{23}Na MQ and ^{23}Na - ^{27}Al D-HMQC MAS NMR spectroscopy. Three different sodium positions, Na I, Na IV, and Na VI, are demonstrated by 1D and 2D ^{23}Na NMR, ^{23}Na - ^{27}Al D-HMQC, and DFT calculation. The distribution of acid centers in different T-sites could be exhaustively calculated by quantificational ^1H NMR and rigorously fitted ^{23}Na MAS NMR. The carbonylation of DME is used to evaluate the $x\text{Na}/(100 - x)\text{H-MOR}$ samples with various acid distributions. The DME conversion rate is linearly proportional to the density of BASs in the T3 site, which proves that the T3 site in the 8-MR of MOR zeolite is the active site for DME carbonylation. It is effective and feasible to explore the acidity of the zeolite by ^{23}Na solid-state NMR such as ^{23}Na MQ and ^{23}Na - ^{27}Al D-HMQC MAS NMR, which could quantitatively map the acid site distribution and further correlate the structure–activity relationship of zeolites. The acidity of the zeolite could be reflected by observing extra-framework cations such as sodium ions, which provides a new insight for the acidity characterization of molecular sieves.

EXPERIMENTAL SECTION

Commercial Na-MOR ($\text{Si}/\text{Al} = 6.5$) was exchanged to $\text{NH}_4\text{-MOR}$ and then anti-exchanged by various concentrations of sodium nitrate solution. ^1H and ^{29}Si experiments were performed on a Bruker Avance III 600 spectrometer equipped with a 14.1 T and 89 mm wide-bore magnet using a 3.2 mm HXY triple resonance MAS probe with the corresponding Larmor frequencies of 600.13 and 119.2 MHz, respectively. The chemical shifts were referenced to adamantane [$\delta(^1\text{H}) = 1.74 \text{ ppm}$] and kaolinite [$\delta(^{29}\text{Si}) = -91.5 \text{ ppm}$], respectively. ^{23}Na MAS NMR and ^{23}Na MQ MAS NMR experiments were performed at a magnetic field of both 14.1 and 18.8 T with the Larmor frequencies of 158.7 and 211.8 MHz, respectively. The chemical shifts were referenced to a 1 M NaCl solution [$\delta(^{23}\text{Na}) = 0 \text{ ppm}$]. ^{23}Na NMR experiments were performed using a 3.2 mm HXY triple resonance MAS probe at 14.1 T and a 3.2 mm HX double resonance MAS probe at 18.8 T. The samples before the measurement of ^1H , ^{27}Al , and ^{23}Na MAS NMR spectra were dehydrated under vacuum ($<10^{-3} \text{ Pa}$) to remove the physisorbed water and then transferred into a glovebox under Ar environment to fill the ZrO_2 rotors with Kel-F caps for further NMR measurements. ^{23}Na - ^{27}Al D-

HMQC experiments were performed on a Bruker Avance III 600 spectrometer equipped with a 14.1 T and 89 mm wide-bore magnet using a 4 mm HX double resonance MAS probe for the triple resonance (^1H - ^{23}Na - ^{27}Al) experiment by using a REDOR-box with the spinning at 10 kHz. Detailed descriptions of the sample preparations, characterization methods, NMR experiments, catalytic testing, and DFT calculation are listed in the [Supporting Information](#).

■ ASSOCIATED CONTENT

SI Supporting Information

The Supporting Information is available free of charge at <https://pubs.acs.org/doi/10.1021/acs.jpcllett.2c00932>.

Zeolite sample preparation, catalytic reaction conditions, DFT calculation, details of NMR experiments, SEM image, XRD patterns, ^1H MAS NMR, ^{27}Al MAS NMR, ^{29}Si MAS NMR, and ^{27}Al MQ MAS NMR spectra, ^{23}Na quadrupolar parameters, isotropic chemical shifts, and quantitative data of sodium ions and BASs in a series of MOR samples ([PDF](#))

Transparent Peer Review report available ([PDF](#))

■ AUTHOR INFORMATION

Corresponding Author

Shutao Xu – National Engineering Research Center of Lower-Carbon Catalysis Technology, Dalian National Laboratory for Clean Energy, iChEM (Collaborative Innovation Center of Chemistry for Energy Materials), Dalian Institute of Chemical Physics, Chinese Academy of Sciences, Dalian 116023, China; orcid.org/0000-0003-4722-8371; Email: xushutao@dicp.ac.cn

Authors

Benhan Fan – National Engineering Research Center of Lower-Carbon Catalysis Technology, Dalian National Laboratory for Clean Energy, iChEM (Collaborative Innovation Center of Chemistry for Energy Materials), Dalian Institute of Chemical Physics, Chinese Academy of Sciences, Dalian 116023, China; University of Chinese Academy of Sciences, Beijing 100049, P. R. China

Wenna Zhang – National Engineering Research Center of Lower-Carbon Catalysis Technology, Dalian National Laboratory for Clean Energy, iChEM (Collaborative Innovation Center of Chemistry for Energy Materials), Dalian Institute of Chemical Physics, Chinese Academy of Sciences, Dalian 116023, China

Pan Gao – State Key Laboratory of Catalysis, Dalian Institute of Chemical Physics, Chinese Academy of Sciences, Dalian 116023, P.R. China; orcid.org/0000-0003-4997-6218

Guangjin Hou – State Key Laboratory of Catalysis, Dalian Institute of Chemical Physics, Chinese Academy of Sciences, Dalian 116023, P.R. China; orcid.org/0000-0001-8216-863X

Rongsheng Liu – National Engineering Research Center of Lower-Carbon Catalysis Technology, Dalian National Laboratory for Clean Energy, iChEM (Collaborative Innovation Center of Chemistry for Energy Materials), Dalian Institute of Chemical Physics, Chinese Academy of Sciences, Dalian 116023, China; University of Chinese Academy of Sciences, Beijing 100049, P. R. China

Yingxu Wei – National Engineering Research Center of Lower-Carbon Catalysis Technology, Dalian National Laboratory

for Clean Energy, iChEM (Collaborative Innovation Center of Chemistry for Energy Materials), Dalian Institute of Chemical Physics, Chinese Academy of Sciences, Dalian 116023, China; orcid.org/0000-0002-0412-1980

Zhongmin Liu – National Engineering Research Center of Lower-Carbon Catalysis Technology, Dalian National Laboratory for Clean Energy, iChEM (Collaborative Innovation Center of Chemistry for Energy Materials), Dalian Institute of Chemical Physics, Chinese Academy of Sciences, Dalian 116023, China; State Key Laboratory of Catalysis, Dalian Institute of Chemical Physics, Chinese Academy of Sciences, Dalian 116023, P.R. China; University of Chinese Academy of Sciences, Beijing 100049, P. R. China; orcid.org/0000-0002-7999-2940

Complete contact information is available at: <https://pubs.acs.org/doi/10.1021/acs.jpcllett.2c00932>

Author Contributions

The manuscript was written through contributions of all authors. All authors have given approval to the final version of the manuscript.

Notes

The authors declare no competing financial interest.

■ ACKNOWLEDGMENTS

This work was supported by the National Natural Science Foundation of China (22022202, 21972142, 21991092, 22002157, and 21991090), the Dalian Outstanding Young Scientist Foundation (2021RJ01), and the National Key R&D Program of China (No. 2021YFA1502600).

■ REFERENCES

- (1) Zhan, E.; Xiong, Z.; Shen, W. Dimethyl Ether Carbonylation over Zeolites. *J. Energy Chem.* **2019**, *36*, 51–63.
- (2) Cheung, P.; Bhan, A.; Sunley, G. J.; Iglesia, E. Selective Carbonylation of Dimethyl Ether to Methyl Acetate Catalyzed by Acidic Zeolites. *Angew. Chem., Int. Ed.* **2006**, *45*, 1617–1620.
- (3) Liu, J.; Xue, H.; Huang, X.; Wu, P.; Huang, S.; Liu, S.; Shen, W. Stability Enhancement of H-Mordenite in Dimethyl Ether Carbonylation to Methyl Acetate by Pre-Adsorption of Pyridine. *Chin. J. Catal.* **2010**, *31*, 729–738.
- (4) Cao, K.; Fan, D.; Li, L.; Fan, B.; Wang, L.; Zhu, D.; Wang, Q.; Tian, P.; Liu, Z. Insights into the Pyridine-Modified MOR Zeolite Catalysts for DME Carbonylation. *ACS Catal.* **2020**, *10*, 3372–3380.
- (5) Li, L.; Wang, Q.; Liu, H.; Sun, T.; Fan, D.; Yang, M.; Tian, P.; Liu, Z. Preparation of Spherical Mordenite Zeolite Assemblies with Excellent Catalytic Performance for Dimethyl Ether Carbonylation. *ACS Appl. Mater. Interfaces* **2018**, *10*, 32239–32246.
- (6) Liu, R.; Fan, B.; Zhang, W.; Wang, L.; Qi, L.; Wang, Y.; Xu, S.; Yu, Z.; Wei, Y.; Liu, Z. Increasing the Number of Aluminum Atoms in T3 Sites of a Mordenite Zeolite by a Low-Pressure SiCl_4 Treatment to Catalyze Dimethyl Ether Carbonylation. *Angew. Chem., Int. Ed.* **2022**, *61* (18), e202116990.
- (7) Cao, K.; Fan, D.; Gao, M.; Fan, B.; Chen, N.; Wang, L.; Tian, P.; Liu, Z. Recognizing the Important Role of Surface Barriers in MOR Zeolite Catalyzed DME Carbonylation Reaction. *ACS Catal.* **2022**, *12*, 1–7.
- (8) Xue, H.; Huang, X.; Zhan, E.; Ma, M.; Shen, W. Selective Dealumination of Mordenite for Enhancing its Stability in Dimethyl Ether Carbonylation. *Catal. Commun.* **2013**, *37*, 75–79.
- (9) Ma, M.; Huang, X.; Zhan, E.; Zhou, Y.; Xue, H.; Shen, W. Synthesis of Mordenite Nanosheets with Shortened Channel Lengths and Enhanced Catalytic Activity. *J. Mater. Chem. A* **2017**, *5*, 8887–8891.

- (10) Chen, N.; Zhang, J.; Gu, Y.; Zhang, W.; Cao, K.; Cui, W.; Xu, S.; Fan, D.; Tian, P.; Liu, Z. Designed Synthesis of MOR Zeolites using Gemini-Type Bis(Methylpyrrolidinium) Dications as Structure Directing Agents and their DME Carbonylation Performance. *J. Mater. Chem. A* **2022**, *6*, 4883–5230.
- (11) MEIER, W. M. The Crystal Structure of Mordenite (Ptilolite). *Zeitschrift für Krist. - Cryst. Mater.* **1961**, *115*, 439–450.
- (12) Chen, X.; Neidig, M. L.; Tuinstra, R.; Malek, A. Direct Observation of Acetyl Group Formation from the Reaction of CO with Methylated H-MOR by In Situ Diffuse Reflectance Infrared Spectroscopy. *J. Phys. Chem. Lett.* **2010**, *1*, 3012–3015.
- (13) Zhou, H.; Zhu, W.; Shi, L.; Liu, H.; Liu, S. In Situ DRIFT Study of Dimethyl Ether Carbonylation to Methyl Acetate on H-Mordenite. *J. Mol. Catal. A Chem.* **2016**, *417*, 1–9.
- (14) Li, B.; Xu, J.; Han, B.; Wang, X.; Qi, G.; Zhang, Z.; Wang, C.; Deng, F. Insight Into Dimethyl Ether Carbonylation Reaction over Mordenite Zeolite from In-Situ Solid-State NMR Spectroscopy. *J. Phys. Chem. C* **2013**, *117*, 5840–5847.
- (15) He, T.; Liu, X.; Xu, S.; Han, X.; Pan, X.; Hou, G.; Bao, X. Role of 12-Ring Channels of Mordenite in DME Carbonylation Investigated by Solid-State NMR. *J. Phys. Chem. C* **2016**, *120*, 22526–22531.
- (16) Boronat, M.; Martínez-Sánchez, C.; Law, D.; Corma, A. Enzyme-Like Specificity in Zeolites: a Unique Site Position in Mordenite for Selective Carbonylation of Methanol and Dimethyl Ether with CO. *J. Am. Chem. Soc.* **2008**, *130*, 16316–16323.
- (17) Chu, Y.; Lo, A.; Wang, C.; Deng, F. Origin of High Selectivity of Dimethyl Ether Carbonylation in the 8-Membered Ring Channel of Mordenite Zeolite. *J. Phys. Chem. C* **2019**, *123*, 15503–15512.
- (18) Rasmussen, D. B.; Christensen, J. M.; Temel, B.; Studt, F.; Moses, P. G.; Rossmeisl, J.; Riisager, A.; Jensen, A. D. Reaction Mechanism of Dimethyl Ether Carbonylation to Methyl Acetate over Mordenite—a Combined DFT/Experimental Study. *Catal. Sci. Technol.* **2017**, *7*, 1141–1152.
- (19) Liu, Z.; Yi, X.; Wang, G.; Tang, X.; Li, G.; Huang, L.; Zheng, A. Roles of 8-Ring and 12-Ring Channels in Mordenite for Carbonylation Reaction: From the Perspective of Molecular Adsorption and Diffusion. *J. Catal.* **2019**, *369*, 335–344.
- (20) Chen, W.; Li, G.; Yi, X.; Day, S. J.; Tarach, K. A.; Liu, Z.; Liu, S.-B.; Edman Tsang, S. C.; Góra-Marek, K.; Zheng, A. Molecular Understanding of the Catalytic Consequence of Ketene Intermediates under Confinement. *J. Am. Chem. Soc.* **2021**, *143*, 15440–15452.
- (21) Bhan, A.; Allian, A. D.; Sunley, G. J.; Law, D. J.; Iglesia, E. Specificity of Sites Within Eight-Membered Ring Zeolite Channels for Carbonylation of Methyls to Acetyls. *J. Am. Chem. Soc.* **2007**, *129*, 4919–4924.
- (22) Bhan, A.; Iglesia, E. A Link Between Reactivity and Local Structure in Acid Catalysis on Zeolites. *Acc. Chem. Res.* **2008**, *41*, 559–567.
- (23) Cheung, P.; Bhan, A.; Sunley, G. J.; Law, D. J.; Iglesia, E. Site Requirements and Elementary Steps in Dimethyl Ether Carbonylation Catalyzed by Acidic Zeolites. *J. Catal.* **2007**, *245*, 110–123.
- (24) Li, Y.; Sun, Q.; Huang, S.; Cheng, Z.; Cai, K.; Lv, J.; Ma, X. Dimethyl Ether Carbonylation over Pyridine-Modified MOR: Enhanced Stability Influenced by Acidity. *Catal. Today* **2018**, *311*, 81–88.
- (25) Gounder, R.; Iglesia, E. Catalytic Consequences of Spatial Constraints and Acid Site Location for Monomolecular Alkane Activation on Zeolites. *J. Am. Chem. Soc.* **2009**, *131*, 1958–1971.
- (26) Jiao, F.; Pan, X.; Gong, K.; Chen, Y.; Li, G.; Bao, X. Shape-Selective Zeolites Promote Ethylene Formation from Syngas via a Ketene Intermediate. *Angew. Chem., Int. Ed.* **2018**, *57*, 4692–4696.
- (27) Yi, X.; Xiao, Y.; Li, G.; Liu, Z.; Chen, W.; Liu, S.-B.; Zheng, A. From One to Two: Acidic Proton Spatial Networks in Porous Zeolite Materials. *Chem. Mater.* **2020**, *32*, 1332–1342.
- (28) Cheng, Z.; Huang, S.; Li, Y.; Cai, K.; Wang, Y.; Wang, M. Y.; Lv, J.; Ma, X. Role of Bronsted Acid Sites within 8-MR of Mordenite in the Deactivation Roadmap for Dimethyl Ether Carbonylation. *ACS Catal.* **2021**, *11*, 5647–5657.
- (29) Zheng, A.; Zhang, H.; Chen, L.; Yue, Y.; Ye, C.; Deng, F. Relationship Between ^1H Chemical Shifts of Deuterated Pyridinium Ions and Brønsted Acid Strength of Solid Acids. *J. Phys. Chem. B* **2007**, *111*, 3085–3089.
- (30) Veeffkind, V. A.; Smidt, M. L.; Lercher, J. A. On the Role of Strength and Location of Brønsted Acid Sites for Ethylamine Synthesis on Mordenite Catalysts. *Appl. Catal., A-Gen.* **2000**, *194*, 319–332.
- (31) Yi, X.; Liu, K.; Chen, W.; Li, J.; Xu, S.; Li, C.; Xiao, Y.; Liu, H.; Guo, X.; Liu, S.-B.; Zheng, A. Origin and Structural Characteristics of Tri-Coordinated Extra-Framework Aluminum Species in Dealuminated Zeolites. *J. Am. Chem. Soc.* **2018**, *140*, 10764–10774.
- (32) Yi, X.; Ko, H. H.; Deng, F.; Liu, S.-B.; Zheng, A. Solid-State ^{31}P NMR Mapping of Active Centers and Relevant Spatial Correlations in Solid Acid Catalysts. *Nat. Protoc.* **2020**, *15*, 3527–3555.
- (33) Zheng, A.; Liu, S.-B.; Deng, F. ^{31}P NMR Chemical Shifts of Phosphorus Probes as Reliable and Practical Acidity Scales for Solid and Liquid Catalysts. *Chem. Rev.* **2017**, *117*, 12475–12531.
- (34) Wang, C.; Dai, W.; Wu, G.; Guan, N.; Li, L. Application of Ammonia Probe-Assisted Solid-State NMR Technique in Zeolites and Catalysis. *Magn. Reson. Lett.* **2022**, *2*, 28–37.
- (35) Huo, H.; Peng, L.; Gan, Z.; Grey, C. P. Solid-State MAS NMR Studies of Brønsted Acid Sites in Zeolite H-Mordenite. *J. Am. Chem. Soc.* **2012**, *134*, 9708–9720.
- (36) Gong, K.; Liu, Z.; Liang, L.; Zhao, Z.; Guo, M.; Liu, X.; Han, X.; Bao, X.; Hou, G. Acidity and Local Confinement Effect in Mordenite Probed by Solid-State NMR Spectroscopy. *J. Phys. Chem. Lett.* **2021**, *12*, 2413–2422.
- (37) Schlenker, J. L.; Pluth, J. J.; Smith, J. V. Positions of Cations and Molecules in Zeolites with the Mordenite-Type Framework. VIII Dehydrated Sodium-Exchanged Mordenite. *Mater. Res. Bull.* **1979**, *14*, 751–758.
- (38) Devautour, S.; Henn, F.; Giuntini, J. C.; Zanchetta, J. V.; Vanderschueren, J. TSDC Relaxation Map Analysis in a Na-Mordenite Zeolite. *Solid State Ionics* **1999**, *122*, 105–111.
- (39) Debras, G.; Gourgue, A.; Nagy, J. B.; De Clippeleir, G. High Power Solid State ^{27}Al , ^{23}Na and ^{29}Si N.M.R. of Precursors and Calcined Samples. *Zeolites* **1986**, *6*, 161–168.
- (40) Jelinek, R.; Özkar, S.; Ozin, G. A. Extraframework Sodium Cation Sites in Sodium Zeolite Y Probed by ^{23}Na Double-Rotation NMR. *J. Am. Chem. Soc.* **1992**, *114*, 4907–4908.
- (41) Smith, L. J.; Eckert, H.; Cheetham, A. K. Potassium Cation Effects on Site Preferences in the Mixed Cation Zeolite Li, Na-Chabazite. *Chem. Mater.* **2001**, *13*, 385–391.
- (42) Lim, K. H.; Grey, C. P. Characterization of Extra-Framework Cation Positions in Zeolites NaX and NaY with Very Fast ^{23}Na MAS and Multiple Quantum MAS NMR Spectroscopy. *J. Am. Chem. Soc.* **2000**, *122*, 9768–9780.
- (43) Hunger, M.; Sarv, P.; Samoson, A. Two-Dimensional Triple-Quantum ^{23}Na MAS NMR Spectroscopy of Sodium Cations in Dehydrated Zeolites. *Solid State Nucl. Magn. Reson.* **1997**, *9*, 115–120.
- (44) Wang, Z.; Chu, W.; Zhao, Z.; Liu, Z.; Chen, H.; Xiao, D.; Gong, K.; Li, F.; Li, X.; Hou, G. The Role of Organic and Inorganic Structure-Directing Agents in Selective Al Substitution of Zeolite. *J. Phys. Chem. Lett.* **2021**, *12*, 9398–9406.
- (45) Barras, J.; Klinowski, J.; McComb, D. W. ^{27}Al and ^{29}Si Solid-State NMR Studies of Dealuminated Mordenite. *J. Chem. Soc. Faraday Trans.* **1994**, *90*, 3719–3723.
- (46) Korfyni, T. I.; Vinek, H.; Nagy, J. B. Characterization of Aluminium Siting in MOR and BEA Zeolites by ^{27}Al , ^{29}Si NMR and FTIR Spectroscopy. *Stud. Surf. Sci. Catal.* **2005**, *158*, 765–772.
- (47) Chen, T. H.; Wouters, B. H.; Grobet, P. J. Aluminium Coordinations in Zeolite Mordenite by ^{27}Al Multiple Quantum MAS NMR Spectroscopy. *Eur. J. Inorg. Chem.* **2000**, *2000*, 281–285.
- (48) Reule, A. A. C.; Sawada, J. A.; Semagina, N. Effect of Selective 4-Membered Ring Dealumination on Mordenite-Catalyzed Dimethyl Ether Carbonylation. *J. Catal.* **2017**, *349*, 98–109.
- (49) Ban, S.; Van Laak, A. N. C.; Landers, J.; Neimark, A. V.; De Jongh, P. E.; De Jong, K. P.; Vlucht, T. J. H. Insight into the Effect of

Dealumination on Mordenite Using Experimentally Validated Simulations. *J. Phys. Chem. C* **2010**, *114*, 2056–2065.

(50) Freude, D.; Hunger, M.; Pfeifer, H. Study Of Brønsted Acidity Of Zeolites Using High-Resolution Proton Magnetic Resonance with Magic-Angle Spinning. *Chem. Phys. Lett.* **1982**, *91*, 307–310.

(51) Pfeifer, H.; Freude, D.; Hunger, M. Nuclear Magnetic Resonance Studies on The Acidity of Zeolites and Related Catalysts. *Zeolites* **1985**, *5*, 274–286.

(52) Freude, D.; Hunger, M.; Pfeifer, H. ^1H MAS NMR Studies on the Acidity of Zeolites. *Chem. Phys. Lett.* **1986**, *128*, 62–66.

(53) Klinowski, J. Solid-State NMR Studies of Molecular Sieve Catalysts. *Chem. Rev.* **1991**, *91*, 1459–1479.

(54) Chu, P. The Deammoniation Reaction of Ammonium Y Zeolite. *J. Catal.* **1976**, *43*, 346–352.

(55) Prilipko, A. I.; Il'in, V. G.; Turutina, N. V.; Nazarenko, V. A.; Mel'nichenko, G. N. Thermographic and Mass Spectrometric Study on Zeolite Dehydration and Deammoniation. *Theor. Exp. Chem.* **1990**, *25*, 467–470.

(56) Xin, S.; Wang, Q.; Xu, J.; Feng, N.; Li, W.; Deng, F. Heteronuclear Correlation Experiments Of ^{23}Na - ^{27}Al in Rotating Solids. *Solid State Nucl. Magn. Reson.* **2017**, *84*, 103–110.

(57) Sklenak, S.; Dědeček, J.; Li, C.; Wichterlová, B.; Gábová, V.; Sierka, M.; Sauer, J. Aluminum Siting in Silicon-Rich Zeolite Frameworks: A Combined High-Resolution ^{27}Al NMR Spectroscopy and Quantum Mechanics/Molecular Mechanics Study of ZSM-5. *Angew. Chem., Int. Ed.* **2007**, *46*, 7286–7289.

(58) Sklenak, S.; Dědeček, J.; Li, C.; Wichterlová, B.; Gábová, V.; Sierka, M.; Sauer, J. Aluminium Siting in the ZSM-5 Framework by Combination of High Resolution ^{27}Al NMR and DFT/MM Calculations. *Phys. Chem. Chem. Phys.* **2009**, *11*, 1237–1247.

(59) Vjunov, A.; Fulton, J. L.; Huthwelker, T.; Pin, S.; Mei, D.; Schenter, G. K.; Govind, N.; Camaioni, D. M.; Hu, J. Z.; Lercher, J. A. Quantitatively Probing the Al Distribution in Zeolites. *J. Am. Chem. Soc.* **2014**, *136*, 8296–8306.

(60) Dedeczek, J.; Lucero, M. J.; Li, C.; Gao, F.; Klein, P.; Urbanova, M.; Tvaruzkova, Z.; Sazama, P.; Sklenak, S. Complex Analysis of the Aluminum Siting in the Framework of Silicon-Rich Zeolites. A Case Study on Ferrierites. *J. Phys. Chem. C* **2011**, *115*, 11056–11064.

(61) Holzinger, J.; Nielsen, M.; Beato, P.; Brogaard, R. Y.; Buono, C.; Dyballa, M.; Falsig, H.; Skibsted, J.; Svelle, S. Identification of Distinct Framework Aluminum Sites in Zeolite ZSM-23: a Combined Computational and Experimental ^{27}Al NMR Study. *J. Phys. Chem. C* **2019**, *123*, 7831–7844.

(62) Takaishi, T.; Kato, M.; Itabashi, K. Determination of the Ordered Distribution of Aluminum Atoms in a Zeolitic Framework. Part II. *Zeolites* **1995**, *15*, 21–32.

(63) Takaishi, T.; Kato, M. Stability of the Al-O-Si-O-Al Linkage in a Zeolitic Framework. *J. Phys. Chem.* **1994**, *98*, 5742–5743.

(64) Fyfe, A. C.; Gobbi, C. G.; Murphy, J. W.; Ozubko, S. R.; Slack, A. D. Investigation of the Factors Affecting the ^{29}Si MAS NMR Linewidths of Zeolites. *Chem. Lett.* **1983**, *12*, 1547–1550.

(65) Tyburce, B.; Kappenstein, C.; Cartraud, P.; Garnier, E. Effects of Exchangeable Cations on the Adsorption Properties of Na^+ Mordenite. *J. Chem. Soc. Faraday Trans.* **1991**, *87*, 2849–2853.

(66) Alberti, A. Location of Brønsted Sites in Mordenite. *Zeolites* **1997**, *19*, 411–415.

(67) Jeffroy, M.; Nieto-Draghi, C.; Boutin, A. New Molecular Simulation Method to Determine both Aluminum and Cation Location in Cationic Zeolites. *Chem. Mater.* **2017**, *29*, 513–523.

(68) Dominguez-Soria, V. D.; Calaminici, P.; Goursot, A. Theoretical Study of The Structure and Properties of Na-MOR and H-MOR Zeolite Models. *J. Chem. Phys.* **2007**, *127*, 154710.

Recommended by ACS

Acid Sites of Phosphorus-Modified Zeolites

Gaurav Kumar, Omar A. Abdelrahman, *et al.*

JULY 23, 2021
ACS CATALYSIS

READ 

Influence of Trimethylphosphine Oxide Loading on the Measurement of Zeolite Acidity by Solid-State NMR Spectroscopy

Yongxiang Wang, Feng Deng, *et al.*

APRIL 22, 2021
THE JOURNAL OF PHYSICAL CHEMISTRY C

READ 

Distribution of Aluminum Species in Zeolite Catalysts: ^{27}Al NMR of Framework, Partially-Coordinated Framework, and Non-Framework Moieties

Kuizhi Chen, Jeffery L. White, *et al.*

APRIL 21, 2021
JOURNAL OF THE AMERICAN CHEMICAL SOCIETY

READ 

What Is Being Measured with P-Bearing NMR Probe Molecules Adsorbed on Zeolites?

Carlos Bornes, Luís Mafra, *et al.*

AUGUST 19, 2021
JOURNAL OF THE AMERICAN CHEMICAL SOCIETY

READ 

Get More Suggestions >